Fourteenth USA/Europe Air Traffic Management Research and Development Seminar (ATM2021)

Aircraft Performance-optimized Departure Flights Using Traffic Flow Funnels

Martin Lindner, Thomas Zeh, Hannes Braßel, and Hartmut Fricke
Chair of Air Transport Technology and Logistics
Technische Universität Dresden
Dresden, Germany
Martin_Lindner@tu-dresden.de

***Abstract*—Aircraft departures often follow standardized and restrictive routes intended to guarantee a safe transition to the en-route network. These procedures are designed usually for various aircraft types, but often without considering the individually optimized flight intents. This paper presents an approach where flights can fly their optimal profile within a procedural space based on actual flight performance to replace standard routes. For this, an algorithm based on DBSCAN identifies typical traffic flow funnels for both a set of radar tracks and individually optimized flight trajectories. For the latter, a 3D pathfinding grid is developed, which expands dynamically using the specific flight performance of the aircraft type. A set of funnels is created along a mean trajectory, which begins at the runway and provides a restricted space for individual trajectory optimization. The procedure is applied exemplary for Munich Airport, where the size of the funnels and the associated fuel-saving potential are determined. The results indicate an average fuel-saving potential of 0.4% with regard to the trip fuel.**

***Keywords*—Trajectory Optimization; Traffic Flow Funnels; Trajectory Clustering; Terminal Maneuvering Area; Departure Management**

I. Introduction

With typically high traffic density and constrained departure and arrival procedures traffic following noise and environmental mitigation, the Terminal Manoeuvring Area (TMA) is an airspace volume in which trajectory optimization is a tedious task and, thus, often omitted. Yet, the procedures force flights often far off their optimal path and profile and into adverse wind conditions. Accordingly, the potential for optimization in the TMA is vast, despite the contrary interests of aviation stakeholders and residents. We propose a method to create departure funnels for aircraft that permit optimization in contained volumes while prohibiting completely arbitrary flight paths to maintain predictability for Air Traffic Control (ATC). Unlike the conventional Standard Instrument Departure (SID), a funnel additionally defines aspect ratios in all dimensions to allow for optimized climb profiles considering individual flight performance, e.g., for following the Continuous Climb Operation (CCO) concept of International Civil Aviation Organization (ICAO) [1]. Since the climb profile is impacted by the aircraft-specific flight performance, including varying gross masses and weather forecasts, the design of funnels requires a smart design methodology to incorporate these uncertainty sources. The traffic flow funnels are built from clustered trajectories, either using radar tracks or individually optimized flights.

The funnel algorithm is based on an iterative clustering consisting of a combined Density-Based Spatial Clustering of Applications with Noise (DBSCAN) [2] and Nearest Neighbor assignment and a secondary DBSCAN within the first iterated cluster. Then, the convex hull of the funnel is computed at equally spaced intervals in the cross-sections of the clustered trajectories and represented by a grid of potential waypoints. Finally, the funnel design algorithm is applied to two data sets to compare funnels based on radar tracks with funnels created from optimized trajectories.

The trajectory optimization, both used for funnel design and finding optimum paths within the funnels, builds upon our established simulation environment TOolchain for Multi-criteria Aircraft Trajectory Optimization (TOMATO) [3], which can consider multiple criteria for optimization including fuel burn, wind, contrails, or airspace restrictions.

For the reference scenario, recorded Automatic Dependent Surveillance – Broadcast (ADS-B) track data from Munich Airport (MUC) is used to build funnels that inherit the current procedures and the resulting flight profiles, as shown in Fig. 1. Using the destinations taken from the recorded ADS-B data, these flights are optimized towards minimum fuel burn without route restrictions with TOMATO consid-

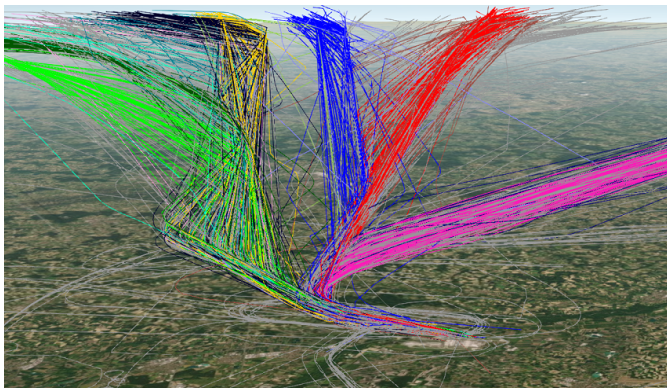

Figure 1: Clustered ADS-B radar tracks of departing flights using runway 26R at Munich Airport. Colors represent clusters where grey flights are outliers.

ering the typical uncertainty sources, such as gross mass and wind, during the climb. Then, the funnel algorithm is applied to these optimized trajectories to form traffic flow funnels enabling optimal flight profiles. Finally, the fuel-saving potential of these performance-optimized funnels is compared to the reference scenario.

II. State of the Art

A. Towards 3D Trajectory Optimization

Trajectory optimization for the entire flight is a vivid research area, where several approaches have been developed to balance multiple optimization objectives such as minimum fuel flow, minimum time, or minimum climate impact by reducing contrail formation [4, 5]. For the operational cost assessment, specific flight performance modeling is crucial for each aircraft-engine combination, including aerodynamics and combustion models. A widely used database for this task is the EUROCONTROL Base of Aircraft Data (BADA) [6]. Due to the mathematical complexity of a flight performance model, the typical approach in trajectory optimization is to split lateral pathfinding from vertical profile calculation [3, 7, 8]. Thus, the cost-optimal path is searched only at cruising altitudes, where the aircraft remains the majority of the flight time. In a consecutive step, the flight profile is optimized on the given flight path. This process is often performed iteratively to find the optimal combination of flight path and profile successively. However, certain approaches for 3D pathfinding have been explored, although being limited mostly to the cruise phase. Hartjes et al. [5] used optimal control with the Radau pseudospectral method to perform a 3D optimization to avoid contrail-inducing regions vertically. Murrieta-Mendoza et al. [9] used a modified Floyd-Warshall algorithm for 3D path optimization in a grid with a 7.5° lateral and a 1000 ft vertical resolution to find optimal cruising conditions, considering the costs required to change altitudes with BADA. Focusing on departing flights, the optimization is either done in regard to an optimal flight profile, which is the CCO [10], or concerning optimizing the procedures and the related ATC interaction in the TMA [11]. Another factor in the ground proximity of the TMA is noise, which Tian et al. [12] consider in an arrival fix allocation problem for Continuous Descent Approach (CDO) arrivals.

B. Sources of Trajectory Uncertainty During Climb

A central challenge during the climb is the individual nature of the vertical profile, which does not only differ among aircraft types but is also affected by various uncertainty sources [13]. Additionally, the characteristics of these uncertainty sources cannot be extracted directly from ADS-B data and, therefore, require additional estimation or analysis. Zeh et al. [14] analyzed the impact of the take off mass with an altitude-dependent optimal True Air Speed (TAS) to find that the resulting vertical trajectory uncertainty is mainly attributed to the mass uncertainty, while an interdependent combination of the mass and the speed intent influences the along-track uncertainty. Alligier [15] used a neural network trained on ADS-B data to estimate mass and speed intents for climbing aircraft as Gaussian distributions, identifying the transitions between speed intents among the uncertainty sources besides mass and the speed intents itself. These speed intent transitions, originating in the cross-over from constant Calibrated Air Speed (CAS) at lower altitudes to constant Mach number at higher altitudes, induce additional trajectory uncertainty [16]. Another relevant uncertainty factor is the thrust, since aircraft operators may reduce the thrust from the typically assumed maximum climb thrust rating of BADA [6]. Sun et al. [17] applied a particle filter to ADS-B data to estimate mass and thrust, which showed that the derated thrust's impact is smaller than the mass.

Besides the aircraft-specific uncertainty sources, the local and temporal variations of the atmospheric parameters, like wind, temperature, and pressure, are the central source of trajectory uncertainty. Zheng and Zhao [18] developed a stochastic model to derive wind, temperature, and pressure uncertainties from the rapid update circle forecasting model. Cheung et al. [19] compared various numerical weather forecasting models to form a large ensemble of forecasts to quantify the weather-related uncertainty sources. Franco et al. [8] also used ensemble weather forecasts to quantify weather uncertainty, which is then used in a Mixed-Integer Linear Programming algorithm to calculate an optimal path with minimized flight time and dispersion. Wan et al. [20] show an optimization for environmentally and fuel-efficient vertical procedure with a multiobjective genetic algorithm, where aircraft mass, time restrictions, and wind affect the optimal trajectory the most.

C. Trajectory Clustering and Traffic Flow Funnels

Trajectory clustering is a field of research that has grown rapidly in recent years with the large-scale storage of ADS-B data. Two unsupervised clustering methods have become commonly accepted for clustering historical flight data, k-means [21] and DBSCAN [2]. Both clustering methods can assign a set of data points into clusters based on similar information. For this particular use case, data points belonging to a single trajectory must be kept together in one cluster. For this, typical applications cluster only parts of the trajectory but assign the entire trajectory to the same cluster. K-means requires the number of clusters as a parameter. This allows using prior knowledge from the airspace under investigation as an input parameter, e.g., number of SID. However, k-means is very susceptible to noise and outliers. The large scatter of waypoints in space often results in erroneous allocations and shifted cluster centroids. Therefore, using either DBSCAN or a combination of DBSCAN and k-means are the predominant ways to cluster flight data points. DBSCAN requires two input parameters; the search radius and the minimum number of points to build a cluster. It handles outliers and noise effectively while assigning outliers to an independent cluster.

With the clustered trajectories, information regarding the system behavior is inferred consecutively. For example, Wang et al. [22] used Principle Component Analysis (PCA) and DBSCAN to cluster trajectories and train a neural network for trajectory prediction. Olive and Morio [23] applied DBSCAN with kernel density estimation using the Epanechnikov kernel to cluster trajectories to identify approach procedures at

Toulouse Airport. There, they formed a transition into the aggregated use of single trajectories to describe procedures at the airport TMA. Similar approaches were used before, eg., Gariel et al. [24] applied k-means and DBSCAN to monitor the airspace and assess its complexity. Basora et al. [25] used Hierachical DBSCAN (HDBSCAN) to find that a symmetrized segment-path distance performs better for precise clustering in confined areas (e.g., TMA) than the commonly used Euclidean distance. Corrado et al. [26] developed a weighted distance function for clustering to account for converging and diverging traffic in the TMA. Olive et al. [27] applied various deep learning techniques with autoencoding neural networks to replace standard distance- or similarity-based clustering like DBSCAN, which showed satisfactory results and required additional parameters fitting. These forms of clustering led to one branch where traffic flows are calculated from trajectory data. In this field, Salaün et al. [28] used PCA and DBSCAN to create maps of the local traffic density, potential for conflicts among aircraft, and outlier aircraft not belonging to dominant traffic flows, using an average trajectory called centroid to represent flow funnels. More recently, Eerland et al. [29] applied Gaussian processes to trajectory data to calculate funnels based on the probability of deviation from the mean trajectory, where the parameters were learned with maximum likelihood estimation. Murça et al. [30] developed a DBSCAN framework to learn traffic patterns in the TMA for daily operations assessment. This proved that the patterns of the traffic flows can be determined reliably from radar data.

D. Optimization Inside Traffic Flow Funnels

Organizing traffic inside flow corridors is an operational concept to enable individual profile optimization potential in future air transportation [31]. Studies for this concept are found in particular for the en-route phase, where large corridors are provided for one traffic direction for aircraft to follow their individual optimal trajectory. Lindner et al. [32, 33] showed that corridors derived from weather forecasts uncertainties, as a sub-form of a flow corridor, offer fuel-saving potential with additional optimization during flight. A further design philosophy exists as a concept for CDO, embodied by the ICAO CDO corridor [34], which relies on simulation data for approach trajectories of several aircraft types and a given arrival route. If the traffic situation permits it, different aircraft types with different operating masses are cleared to fly their optimum descent profile. For ensuring minimum separation between aircraft, for example, during CDO, a concept of self-separation is proposed frequently [35–37].

The SIDs for departures, however, are typically standardized routes valid for all aircraft types, which do not offer any flexibility in lateral optimization, although some studies already identified a corresponding fuel-saving and noise abatement potential. Zhou et al. [38] constructed individual arrival and departure routes within the TMA considering different weather scenarios. Ho-Huu et al. [39] showed a multilevel optimization model which combines the design of routes for terminal operations with the route allocation of flights to minimize noise and fuel consumption. Although they show significant fuel (7%) and noise reduction potential (31%) compared to their reference case in Amsterdam Schiphol, their lateral trajectory optimization is still limited to the stringent SID. Chevalier et al. [40] optimized departures using a search graph with integrated altitude restrictions and maximum turn angles. They construct the graph from several rings around the airport, on which nodes are placed at an angular difference of 5° each. This approach shows satisfactory results in avoiding obstacles but includes only a limited vertical profile optimization.

III. Methodology

A. Concept of Performance-optimized Departure Funnels

This paper evaluates the potential benefit of traffic flow funnels regarding the flight efficiency of departing flights. Thus, it emphasizes the generation of such funnels from either historical flight tracks or optimized departure profiles and their comparison regarding an optimization potential. Although the handling and safe control of the traffic flow is vital for operational implementation, the collision risk and safety study will be conducted in one of the upcoming steps, after this fundamental study demonstrated sufficient optimization potential.

Compared to a conventional SID, the funnel defines a spatial corridor that permits lateral and vertical optimization. To achieve the full optimization potential, the funnel must be designed to permit most aircraft types to reach their optimal profile in the presence of typical uncertainty sources, like the variability in the local weather and the actual take off mass. Furthermore, the funnel must also consider obstacle clearance, which is achieved with additional lower bounds where required. The calculation and evaluation of the traffic flow funnels take place in the following four stages:

1) Historical departure flights from ADS-B data are clustered to various funnels incorporating the actual procedures as a reference scenario to identify benefits of the funnel concept;
2) These flights are optimized without any route restriction considering a variety of aircraft types, masses, and weather forecasts using TOMATO with a newly developed search graph. Then, these trajectories are clustered to optimized funnels with the same clustering algorithm;
3) Next, both sets of funnels are simulated with the same historical flight schedule, where the flights are optimized according to the weather data valid for this period but are restricted to fly inside the given funnels only;
4) The flight efficiency of the two funnel sets is compared to quantify the efficiency gain of the optimized funnels.

The optimization is applied in the Extended Terminal Maneuvering Area (E-TMA), which we define as a radius of 100 NM from the aerodrome reference point. Exit points are given either by the end of the funnels when optimizing inside the funnels or by the point where the orthodrome between departure and destination airport intersects with the E-TMA radius for the unrestricted optimization. The aircraft types are

limited to a set of commonly used commercial jet aircraft. Therefore, turboprop aircraft, as well as general or military aviation, are excluded, since their traffic share is neglectable at major European airports.

B. Trajectory Optimization

A two-stage approach is used to find a feasible optimum aircraft trajectory within the E-TMA. In the first stage, an optimum 3D path is calculated in a graph-based on tabulated aircraft performance values of BADA [6]. The vertices of this path are then used for the second stage, where the COmpromized Aircraft performance model with Limited Accuracy (COALA) [41] calculates the aircraft-specific high-resolution climb profile to quantify the flight efficiency.

1) Reduced Aircraft Performance Complexity During Path Finding: The path is calculated in a search graph through virtual nodes in a 3D space connected by edges. The movement of the aircraft along the graph depends on the flight performance, which constantly changes due to acceleration, flight altitude, and over time. However, commonly used shortest path algorithms rely on independent costs for each edge; thus, they cannot maintain the information about the current state of aircraft when moving from one to the next edge. Nevertheless, the edge costs must consider the flight performance required to move the aircraft from node to node. Therefore, the rate of climb ROC, the true airspeed TAS, and the fuel flow FF are assumed to describe the flight performance as best as possible given the limited availability of aircraft state information in the graph search.

For applications where the full Aircraft Performance Model (APM) cannot be used, BADA 4 [6] provides the Performance Table Data (PTD) that contains tabulated flight performance values for most aircraft types. These files are an output of the BADA APM and are calculated in International Standard Atmosphere (ISA) conditions without wind for the standard speed profile of the aircraft type and three classes of typical aircraft masses segregated into the flight phases *climb*, *cruise*, and *descent*. Furthermore, the reduction of aircraft mass due to fuel burn is omitted. With these simplifications, however, the PTD is suitable for the cost calculation in the path search. The parameters, including ROC, TAS, and FF, are provided for a set of $25-30$ flight levels and corresponding pressure altitudes ranging from the ground to the service ceiling. For coverage of all altitudes required in the path search, we interpolate linearly between the values if the required pressure altitude is not available in the file. While the usage of the PTD reduces the path optimization to three masses per aircraft type, the profile calculation is performed individually afterward based on this 3D path with COALA, which is built upon the APM and, thus, provides a high-resolution profile without the limitations from the tabulated values.

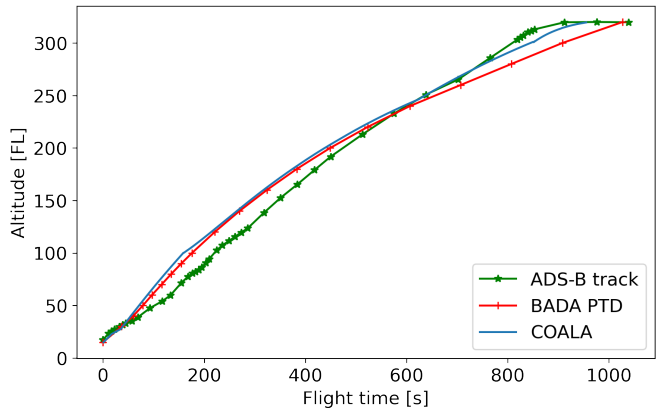

Figure 2: Comparison of the vertical profile from the ADS-B track data (green) with the BADA PTD files (red) and the optimization of COALA (blue) of the same aircraft type.

The fuel burn during climb FB_{cl} is part of the edge costs and is calculated as the integral of altitude-dependent FF over time t, see (1). The altitude h of the aircraft depends on climb time and the ROC, which only depends on the current altitude in the PTD, cf. (2) and (3).

$$FB_{cl} = \int_t FF(h(t))\ dt \tag{1}$$

$$h(t) = \int_t ROC(h)\ dt \tag{2}$$

$$dt = \frac{dh}{ROC(h)} \tag{3}$$

By rearranging (1) to (3), an altitude-dependent FB_{cl} can be calculated (4), which yields the fuel burn required to climb from the current altitude h_1 to the next altitude h_2.

$$FB_{cl} = \int_{h_1}^{h_2} \frac{FF(h)}{ROC(h)}\ dh \tag{4}$$

The climb distance is determined as the integral of TAS over time, see (5). Since the PTD uses ISA conditions, the resulting distance is the still air distance SAD, i.e., without wind effect. The effect of the head and tailwind components is determined utilizing the weather forecast and added to the edge costs with a dedicated wind cost layer [3].

$$SAD = \int_t TAS(h(t))\ dt \tag{5}$$

2) 3D Pathfinding: Using the flight performance calculation described before, an individual search graph is generated to match the performance of the departing aircraft, as shown in Fig. 3. Each node in the graph is described with a unique coordinate $c(\phi, \lambda, h)$ with the latitude ϕ, longitude λ and the altitude h in [°] and [Pa], respectively. The actual position of each node depends on the individual flight performance of the selected aircraft type and mass class from the PTD to ensure that the aircraft can reach each node accordingly.

As parameters for the grid creation, a set of pressure altitudes $\mathbb{A} = \{h_1, h_2, ..., h_n\}$, and an interval angle θ are defined. θ represents the interval of permitted change in flight direction from the previous direction. Therewith, it is ensured that the climb duration between two altitudes from $\mathbb{A}$ is sufficient to turn at least θ with a standard Rate Of Turn (ROT) $\dot{\psi}_s = 3°s^{-1}$. As $\mathbb{A}$ and θ both lead to an exponential growth

of the search path complexity, they must be selected balancing calculation time and accuracy. Any grid generation starts at the selected runway threshold (point I in Fig. 3) and follows the take-off direction until the end of the Take-Off Run Available (TORA) at runway elevation (point II) because the actual take-off distance is unknown in the path search. From point II, a short climb segment continues straight along the extended runway centerline until reaching 100 m above the runway elevation (point III). From there, the search graph is expanded gradually in a conic shape, considering the pressure altitude steps in $\mathbb{A}$ and θ.

Graph expansion in the performance-dependent grid: The expansion of a graph identifies the neighboring nodes from a current node, which uses a grid build from the flight performance of the aircraft PTD. Neighbor nodes are generated dynamically based on the aircraft state at the current node and the available climb performance, see Fig. 3.

Let the current node be located at the coordinate $c(\phi, \lambda, h)$ with the previous flight direction ∇ from where the node was originally created. The grid is expanded from c with the following steps:

1) The first node is placed in the direction of ∇ at the next altitude h_{i+1} to account for a straight climb without direction change. For this, (2) is used to determine the climb duration t_{cl} from h to h_{i+1} to then calculate the SAD_{cl} with (5).
2) Further nodes are added at h_{i+1} using SAD_{cl}, but permitting left and right turns in $n \in \mathbb{N}$ angular steps of θ up to the maximum angular difference $\psi_{max} = \dot{\psi}_s \cdot t_{cl}$ to avoid a ROT that exceeds $\dot{\psi}_s = 3°s^{-1}$.
3) For permitting level segments, additional nodes are inserted at h with turns permitted at n steps of θ up to $\pm\psi_{max}$. Furthermore, SAD_{cl} is used to ensure that these nodes are located perpendicular below the previously inserted nodes.

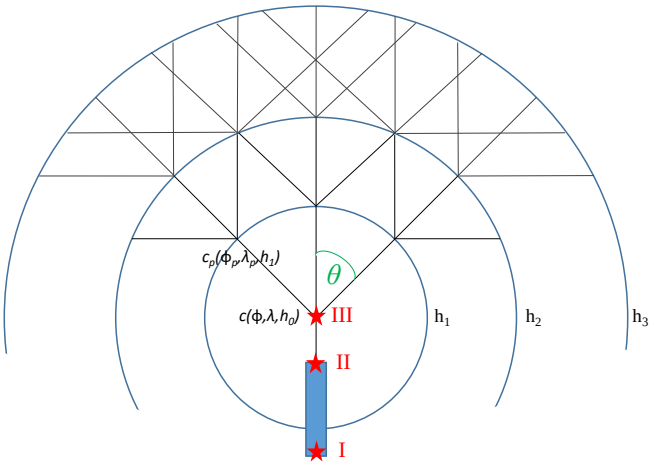

Figure 3: Simplified top view of the 3D path search grid for the climb with $\theta = 45°$, three different optimization altitudes $\mathbb{A} = \{h_1, h_2, h_3\}$. The grid expands at the extended runway centerline of node III, which is also the current node c, resulting in a projected neighbor node c_p.

If the flight direction has been changed, a new flight direction ∇_p for the projected next node must be calculated:

$$\nabla_p = \nabla \pm n \cdot \theta \quad \text{with} \quad |\nabla - \nabla_p| \leq \psi_{max} \tag{6}$$

With SAD_{cl} and ∇_p, a coordinate c_p described by ϕ_p and λ_p for the new node p is calculated using the *Vincenty's Direct Problem* [42]. This procedure ensures that the aircraft can reach all nodes with the given flight performance without exceeding $\dot{\psi}_s$. Descent segments are not intended for the optimized climb and are, therefore, omitted.

Shortest path algorithm: For pathfinding in the graph, the A* search algorithm is used due to its proven completeness, optimality, and efficiency [43]. The A* uses a heuristic that *estimates* costs from the current node to the destination node to guide the search towards the destination without unnecessary graph expansions. As a heuristic, we use 90% of the FB required to reach the destination directly from the current node, thus avoiding over-estimation for the A* to work properly.

The *actual* costs are calculated when visiting the node. The edge cost C is calculated with the FB of the PTD, considering either climb or cruise FB based on the node altitudes. The effect of wind is added to the costs with the headwind component HW at the given location and altitude. A default fuel price FP is assumed for all flights. Eq. (7) describes the calculation of C for a single edge:

$$C = \left(FB + \frac{HW \cdot FB}{TAS} \right) \cdot FP \tag{7}$$

The total actual cost of a node is the sum of the edge cost along the shortest path from the source. The A* minimizes the sum of the actual and estimated costs to find the shortest path to the destination. Fig. 4 shows the obtained costs as an example for a flight using a color palette, where the yellow edges to the north yield lower costs and, therefore, are more efficient to chose than the white edges in the south.

3) Vertical profile with COALA: When the shortest path is found, it is then simulated with the flight performance model COALA [41] to optimize the vertical profile compared to the default speed regime used in the PTD. COALA builds upon the aircraft-specific data provided by BADA versions 3 and 4 and utilizes an advanced approach with a Proportional–Integral–Derivative (PID) controller for each flight phase and a sophisticated engine model for contrail and emission calculation. With this, the speed profile during the climb is optimized by maximizing the climb rate to reach altitudes with reduced fuel burn quickly [10]. The output of COALA is a high-resolution profile with an accurate fuel burn so that the fuel-saving potential is quantified adequately.

C. Clustering Algorithm

We consider a set of trajectories T_i, $i \in \{1, .., I\}$, where I is the number of trajectories under consideration, each represented by a sequence of geographic coordinates P_i^k, where $k \in \mathbb{N}$ is the k^{th} point of the trajectory T_i. P_i^k is defined in three-dimensional airspace by ϕ, λ and their

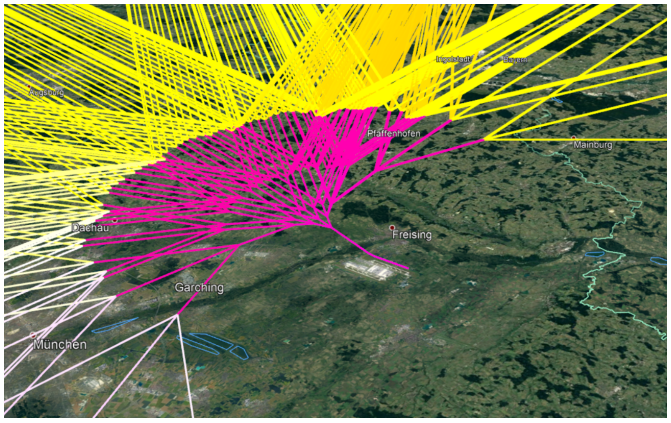

Figure 4: 3D departure search grid from runway 26R to a northern destination with $\theta = 30°$, $\dot{\psi}_s = 3°s^{-1}$ and $\mathbb{A} = \{h_1, ..., h_{12}\}$ optimization altitudes. The color indicates altitude and distance-dependent estimated costs to destination (magenta highest). Map: Google, ©2021, GeoBasis-DE/BKG

altitude in [ft]. The input data is pre-processed to remove unsuitable data. These include inconsistent flight paths, those represented by insufficient data points, and abnormal procedures, e.g., rejected takeoff. Subsequently, the flight paths are truncated at the boundaries of the area under consideration. In the present case, below 300 ft above the airport elevation and at a distance of 100 NM from the airport reference point. For further calculation steps, the geographic data points are transformed into a local Cartesian coordinate system returned as x_{East}, y_{North}, and z_{Up} and augmented by linear interpolation. The origin of the local coordinate system is located at the reference point of the airport.

The first data points P_i^1 of each T_i are assigned to an inner cluster using the nearest neighbor condition to the runway threshold respectively P_i^{end} to an outer cluster assigned by a DBSCAN [2]. Thus, each T_i was assigned to a preliminary cluster $PC_{a,b}$, $a \in \{1, ..., A\}$, $b \in \{1, ..., B\}$, where A is the number of runway thresholds (e.g. $a = 1$ is *26R* of MUC) and B the number of outer cluster resulting from DBSCAN.

Subsequently, it was examined whether flight trajectories T_i exists, deviating from the other flight paths within their preliminary cluster. For this, all P_i^k which are assigned to $PC_{a,b}$ were sorted according to their distance flown. Then, each coordinate $P_i^k(sorted) \in T_i$ within a preliminary cluster $PC_{a,b}$ that deviates more than one local standard deviation from the local mean over a sliding window, were filtered and clustered by a DBSCAN. The entire trajectory T_i was deleted from $PC_{a,b}$ and assigned to new sub-clusters $PC_{a,b}^s$, $s \in \{1, ..., S\}$ where S number of sub-clusters in $PC_{a,b}$. The final clusters C_n equals the sum of $PC_{a,b}$ and $PC_{a,b}^s$. For all C_n that contains a minimum number of T_i, all $P_i^k \in C_n$ were sorted again based on their distance flown. Then, the mean trajectory $\bar{T}_n^p = (x_n^p, y_n^p, z_n^p)$, where p is the p^{th} point along $\bar{T}_n$, of each C_n was calculated over a sliding window across neighboring elements of $P_i^k(sorted) \in C_n$. The calculated $\bar{T}_n^p$ were transformed into evenly spaced trajectory points using a *Modified Akima cubic Hermite interpolation*. Each $P_i^k \in C_n$ was assigned to a trajectory segment $\bar{T}_n^p$ to T_n^{p+1}, using the shortest Euclidean distance. Finally, the upper and lower dimensions of the convex hull were calculated by the maximum and minimum altitude component (z_{Up}) of the Euclidean distance between the assigned data points P_i^k and the Mean Trajectory segment from $\bar{T}_i^k$ to $\bar{T}_i^{k+1}$. The horizontal dimensions were calculated within three times the standard deviation of the horizontal Euclidean distance of P_i^k and the spline segment $\bar{T}_i^k$ to $\bar{T}_i^{k+1}$. Finally, the local Cartesian coordinates were converted into geographic coordinates.

D. 3D Pathfinding Inside the Traffic Flow Funnels

After deriving a traffic flow funnel from clustering, the flights are reoptimized using the same flight performance method according to section III-B. For this, two steps are necessary for each flight from the flight plan. First, the flight is allocated to the funnel that ends closest to the flight's destination. Second, the flight is reoptimized considering the actual weather forecast while being restricted to the selected funnel. For this purpose, an additional 3D funnel grid is developed for the A* different from the grid described in section III-B2.

1) Funnel Allocation to Flights: The funnel for a particular flight is selected for the path search based on the mean coordinate of the last gate, which is closest to the destination airport in terms of the great-circle distance. This assumption may lead to an unbalanced distribution of traffic associated with capacity insufficiency, which will be clarified in later traffic analysis. Alternatively, the funnels might be allocated manually or considering the lengths and curves of the funnel to avoid detours, if desired.

2) Funnel Grid: Each funnel gate consists of coordinates in a uniform grid with α lateral and β vertical sections, as shown in Fig. 5. The resulting planar mesh of the gate consists of available nodes for the A*. All nodes of the next gate $p+1$ are potential neighbors from a node at the current gate p. However, it has to be checked whether the current aircraft can reach the altitude within the available distance $d_{p,p+1}$ between p and $p+1$. Here, the aircraft-specific PTD is used again to calculate the required SAD_{cl} to reach the altitude of the next gate's nodes, cf. (5). Since the target is to climb to the cruise altitude, descents are prohibited in the funnel grid as well. It is not allowed for the pathfinding to skip a gate entirely. However, skipping intermediate altitudes when flying from p to $p+1$ is permitted if the climb performance is sufficient.

E. Evaluation Metrics

The evaluation of the identified funnel areas is performed in two parts. One is the number and size of the determined funnels, and the other is the flight efficiency that will result from a modified funnel scenario. The metrics use common key indicators for aviation.

1) Funnel Dimension: The number of funnels represents both the complexity in traffic assignment and the required procedures to be applied therein. In conjunction with the size of the individual gates, a comparative metric for the

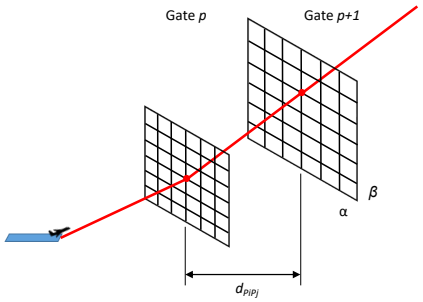

Figure 5: Simplified 3D funnel grid for two rectangular gates p and $p+1$ with $\alpha = 6$ lateral and $\beta = 6$ vertical sections, resulting in 49 grid points for each gate.

use of airspace is given hereby. Additionally, the lateral and horizontal distance of the grid points at each gate is measured, which forms the optimization grid. Based on this, an overview of the precision during the optimization is provided.

2) Flight Efficiency: The efficiency of the flight is measured with the ICAO Global Air Navigation Plan (GANP) [44] Performance Indicator *Route Extension* and with a direct comparison of the fuel consumption. All climb flights are truncated in the same radius used for the clustering and funnel calculation. From there on, a direct flight to the destination is assumed to avoid any other influence on the actual relative fuel savings. The ground distance is used for the route extension metric to consider the impact of wind accordingly.

IV. Results

A. Scenario Definition

The clustering and trajectory optimization steps described in section III are applied for departures at MUC. This airport in the northeast of Munich has a two-runway system with an elevation of 453 m MSL and allows independent parallel runway operations. According to MUC Aeronautical Information Publication (AIP) [45], both runways have published departure routes to a total of 18 en-route waypoints, already enabling flight planning towards the destination with only a few TMA-related detours. As Fig. 8(a) shows, only some of these waypoints are used frequently, which leads to a larger scale of air space usage in the area north of MUC. At the same time, noise abatement measures restrict the arrivals and departures in the south heavily due to the proximity of the urban areas of Munich.

For a comprehensible evaluation and for avoiding interference from traffic in parallel runway operation, this stage of work assumes a facilitated traffic scenario where only one runway with one direction is used. Therefore, the considered procedures are limited to the runway threshold *26R*, which is the main operating direction due to wind, see Fig. 6. Thus, the scenario covers the flights to destinations requiring departures to the northern side of the airport.

The considered ADS-B data set covers flights from 01 to 30 September 2019, so a typical traffic demand for the summer period. The data is pre-filtered concerning its plausibility

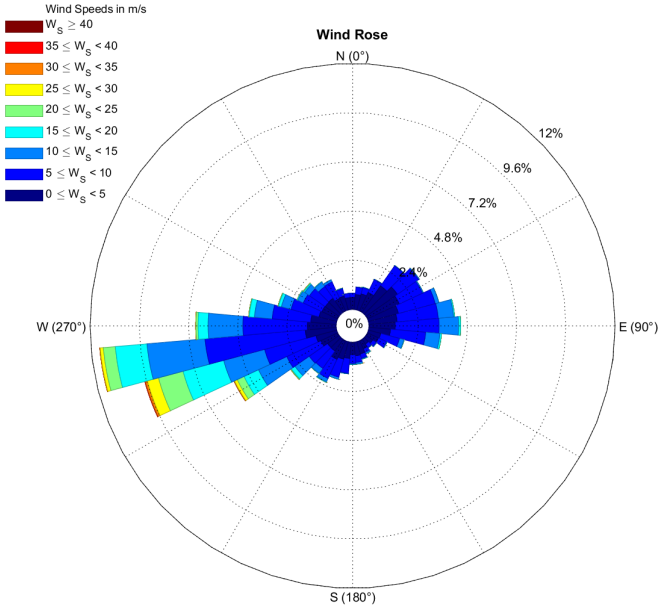

Figure 6: Wind rose for MUC based on METAR data for 2019. The wind direction points towards the center, where the wind is aggregated in segments with intervals of 10° and 5 m/s. The color of each segment represents wind speed and the length of any segment the share of observations.

of a continuous climb. Thus, only flights with at least 25 measurements within a radius of 100 NM around the airport are considered. For the inner clustering, only measurements with a minimum ground speed of 180 kt after the runway end are used. The minimum number of flights to form a cluster is set to 30 and the search radius to $\epsilon = 6000$ km. The mean trajectory of a cluster is formed by a spline consisting of 500 sampling points. Based on this, 40 rectangular gates are determined along the spline that describes the funnel. The width of each gate is divided into $\alpha = 20$ and the height into $\beta = 40$ sections, resulting in 800 grid points for each funnel in the optimization. For the funneling of the optimized trajectories according to section III-B2, the input parameters are mostly identical, although the minimum number of flights per cluster has been reduced to 25, as the clusters would become too wide for efficient flight control otherwise.

In total, approximately 300 departure profiles were calculated inside the ADS-B funnels, depending on the specific traffic volume from the flight schedule. The scheduled flights were allocated to the runways based on the initial bearing between departure and destination airport, where flights between 260° and 90° are selected to depart from the analyzed runway *26R*, which is the northern runway and therefore should handle flights destined to the north of MUC. Different weather scenarios are used to optimize the flights considering typical weather uncertainty in the resulting funnels. We use the weather forecasts corresponding to the flight schedule period, provided by the Global Forecast System (GFS) of the National Oceanic and Atmospheric Administration (NOAA). These weather forecasts are available in GRIB2 format with a lateral resolution of 0.25° four times a day [46]. A further variation

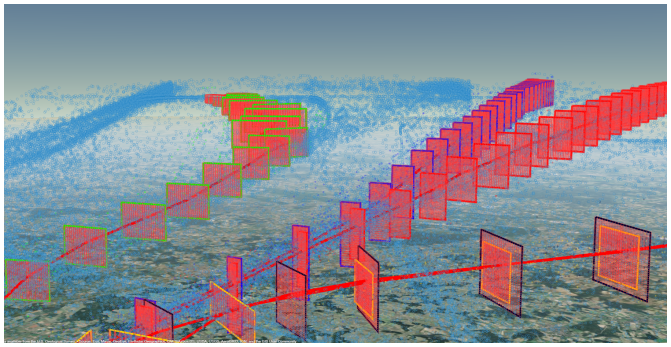

Figure 7: Four of seven 3D departure funnels with rectangular gates (red with unique border colors per funnel) from clustered flight data (09/2020), with the raw ADS-B points (blue), and the mean trajectory per funnel (red lines). Blue points outside funnels are outliers or other runways.

is obtained indirectly from different flight performances of different aircraft types as given in the flight schedule for each day in the investigated period. Each aircraft from the flight schedule is assigned its corresponding BADA 4 aircraft type. For aircraft types without PTD files, the most similar type in terms of aircraft size is chosen. Since the mass of each aircraft is not included in the flight schedule, it is randomly selected from a value between 60% and 90% of the available payload plus fuel mass.

B. Funnels of ADS-B and Optimized Clustered Flights

Fig. 7 depicts four clustered departure procedures and the resulting funnels based on ADS-B tracked flights (blue points, all recorded flights). Apparent is an ascending altitude of the corresponding gates combined with an increase in width and height the further away from the threshold. In total, 1165 flights with valid data for the clustering algorithm departed from threshold *26R* (cluster $a = 1$) were considered. Using these movements, a total of 7 funnels aggregate the major departure directions composed of 40 gates each. Fig. 8(a) displays all clusters and the resulting funnels in a top view. The orientation of the funnels shows that the majority of flights are heading to the west and north. Flights flying to the east are bundled in a single funnel pointing to the north-northeast. A look at the raw data revealed that, in principle, a small number of flights are also heading directly to the east. However, those flights do not reach the minimum number of flights required for a cluster and are excluded accordingly. For these few flights, the flight efficiency will be underestimated as they are constrained by another, less optimal funnel compared to the actual operations.

For the scenario with optimized trajectories using the grid from Section III-B2, 9098 flights were calculated, which resulted in 35 funnels. The higher number of clusters is caused by the diversified flights with a more direct and individual pathing to their destinations, resulting in the fan shape in Fig. 8. Here, the DBSCAN parameters lead to a homogeneous area clustered into parts, as constraints were not applied during the path search. Due to the different number of flights and clusters examined and despite the minimum number of flights per cluster already adjusted, the efficiency comparison is only possible within limits. Additionally, the shape of funnels is also much wider, as flexible route selection and direct routing towards the destination broadens the clusters considerably. In comparison, the flights in the ADS-B funnels converge due to the transition to the en-route network on common waypoints at the end of each SID. For the optimized flights, however, this is not the case. Table I lists an overview of the spatial dimensions of the gates for both scenarios. Since the optimized funnels must be integrated into the existing route network, the funnels could be narrowed significantly by specifying en-route waypoints as optimization targets. Furthermore, the high number of clusters could increase the complexity in traffic handling as well as the separation to approaching traffic flows. A reduction is advised to balance optimization and ATC requirements,e.g., by merging of neighboring clusters. According to Table I, the range of the height of the gates and, accordingly, the vertical extent of the funnels is smaller compared to the ADS-B scenario. This might be due to the limited selection of 15 aircraft was available in TOMATO and COALA, which does not cover the entire flight schedule with 47 different aircraft types. Additionally, idealized thrust and velocity profiles might underestimate the spread in vertical flight performance.

Table I. Dimension of departure funnels and grid point spacing per gate from the ADS-B data and optimized flights.

[m]	Percentile	Gates ADS-B		Gates Opt	
		Size	Spacing	Size	Spacing
Width	0.5	4793	240	10556	528
	0.05	2112	106	1874	94
	0.95	7542	377	19797	989
Height	0.5	2946	73	1719	43
	0.05	1367	34	434	11
	0.95	4612	115	3558	89

Finally, the selected cluster parameters, in particular radius and ϵ for DBSCAN, contribute significantly to the resulting size and number of the funnels. These parameters were determined as a sufficiently good trade-off between size and number of clusters individually per scenario. A quantitative measure of cluster size is proposed in section V.

C. Flight Efficiency

For examining the effects of the optimized funnels on flight efficiency, all flights of the flight schedule are re-optimized in both funnel scenarios, permitting full usage of the funnel dimensions. For the funnels designed from the optimized flights, an average saving of 16 kg per departure is achieved. This corresponds to a value of about 0.4% for the entire flight. The ground distance until the destination is also reduced by 0.5%. The spread of these values is shown in Fig. 9. Although these savings appear rather small, only the first half of the climb phase until FL250 inside the E-TMA was considered for optimization, which averages to a fuel mass of 956 kg and a distance of 108 km in total per flight.

V. Conclusion and Outlook

This work differs from the current ATC procedures for departure and climb profiles following the predefined SID,

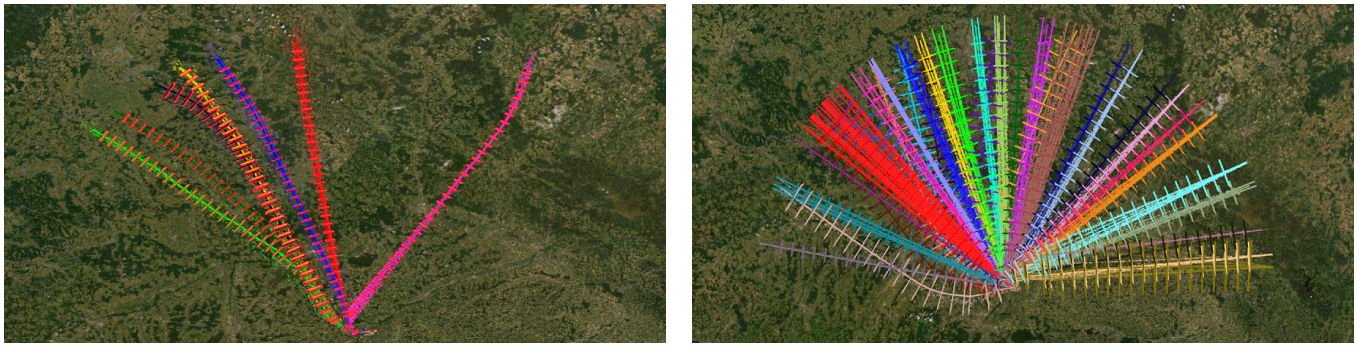

(a) ADS-B radar tracks

(b) TOMATO optimized flights

Figure 8: Clustered flight tracks of departing flights using runway 26R at Munich Airport.

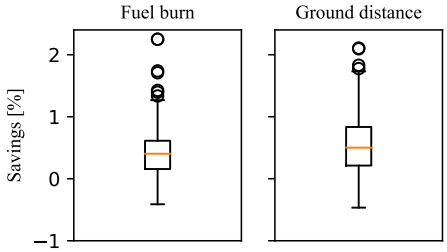

Figure 9: Boxplot of flight efficiency (fuel burn, ground distance) as the result of a transition from ADS-B to optimized calculated departure funnels.

which are replaced by a procedural space entitled traffic flow funnels. Limited to these funnels, aircraft can follow their performance-dependent optimal profile in terms of fuel efficiency. As the beginning of the funnels is always tied to the runway threshold and the end aims at as many flight directions as possible, the resulting shape widens the further away flights are from the threshold, which must be limited to ensure separation between aircraft. A set of funnels allows departures in various directions to minimize the distance to the en-route network. Clustering of ADS-B tracks departing from MUC prove that such funnels already exist with a decent vertical extend, but the lateral spacing is strongly limited due to the SID design. When optimizing these flights with 30 weather scenarios for September 2019, a set of optimized funnels could be created utilizing the same funnel algorithm. While the consistent implementation offers fuel-saving potential, the airspace required for these optimized funnels increased significantly at the same time.

Prior to developing a full traffic concept and the associated safety assessment, the appropriate size and number of the funnels should be studied next. Additionally, the integration of aircraft noise exposure is necessary for lateral pathfinding. The values of parameters are currently selected qualitatively for the funneling algorithm. Next, the parameters must be optimized to maintain the airport capacity, to match the traffic concept of the arrivals, and to ensure a suitable safety level regarding collision risks at all times. This results in another optimization problem, where the traffic flow and the necessary ATC monitoring play an important role. Alternatively, the current SID routes might be widened to funnels instead, thus maintaining the current traffic setup, but offering additional freedom for optimization without compromising capacity and safety much. It should be noted that the ADS-B data contains an unknown share of flights with radar vectors, with might have induced a spread in the ADS-B funnels. However, extensive vectoring far off the SID is excluded with the outlier analysis in the clustering.

While this work explores the fundamental flight efficiency potential of departure funnels, the control and separation assurance both inside funnels and where funnels intersect must be discussed in further steps. Although similar procedural spaces introduced in section II reported positively on self-separation of aircraft, while methods from point merge procedure may also be adapted to the funnels.

References

[1] International Civil Aviation Organization, "Continuous climb operations (cco) manual doc 9993 an/495," tech. rep., 2013.

[2] M. Ester, H.-P. Kriegel, J. Sander, and X. Xu, "A density-based algorithm for discovering clusters in large spatial databases with noise," pp. 226–231, AAAI Press, 1996.

[3] S. Förster, J. Rosenow, M. Lindner, and H. Fricke, "A Toolchain for Optimizing Trajectories Under Real Weather Conditions and Realistic Flight Performance," in *Greener Aviation*, (Brussels), 2016.

[4] J. Rosenow, S. Förster, M. Lindner, and H. Fricke, "Multicriteria-Optimized Trajectories Impacting Today's Air Traffic Density, Efficiency, and Environmental Compatibility," *Journal of Air Transportation*, vol. 27, pp. 8–15, Jan. 2019.

[5] S. Hartjes, T. Hendriks, and D. Visser, "Contrail Mitigation Through 3D Aircraft Trajectory Optimization," in *16th AIAA Aviation Technology, Integration, and Operations Conference*, AIAA AVIATION Forum, American Institute of Aeronautics and Astronautics, June 2016.

[6] A. Nuic, D. Poles, and V. Mouillet, "Bada: An advanced aircraft performance model for present and future atm systems," *International Journal of Adaptive Control and Signal Processing*, vol. 24, no. 10, pp. 850–866, 2010.

[7] R. Félix Patrón and R. Botez, "Flight Trajectory Optimization Through Genetic Algorithms for LNAV and VNAV Integrated Paths," *Journal of Aerospace Information Systems*, vol. 12, Sept. 2015.

[8] A. Franco, D. Rivas, and A. Valenzuela, "Optimal Aircraft Path Planning in a Structured Airspace Using Ensemble Weather Forecasts," in *8th SESAR Innovation Days*, (Salzburg), 2018.

[9] A. Murrieta-Mendoza, C. Romain, and R. M. Botez, "3d cruise trajectory optimization inspired by a shortest path algorithm," *Aerospace*, vol. 7, p. 99, Jul 2020.

[10] J. Rosenow, S. Förster, and H. Fricke, "Continuous Climb Operations with Minimum Fuel Burn," in *SESAR Innovation Days*, (Delft), 2016.

[11] M. Liang, *Aircraft Route Network Optimization in Terminal Maneuvering Area*. PhD thesis, Université de Toulouse, Toulouse, 2018.

[12] Y. Tian, L. Wan, K. Han, and B. Ye, "Optimization of terminal airspace operation with environmental considerations," *Transportation Research Part D: Transport and Environment*, vol. 63, pp. 872–889, Aug. 2018.
[13] S. Mondoloni, "Aircraft trajectory prediction errors: Including a summary of error sources and data, FAA/Eurocontrol Action Plan 16," Tech. Rep. 2, 2006.
[14] T. Zeh, J. Rosenow, and H. Fricke, "Interdependent Uncertainty Handling in Trajectory Prediction," *Aerospace*, vol. 6, p. 15, Feb. 2019.
[15] R. Alligier, "Predictive Distribution of the Mass and Speed Profile to Improve Aircraft Climb Prediction," in *13th USA/Europe Air Traffic Management Research and Development Seminar (ATM2019)*, (Vienna), June 2019.
[16] T. Zeh, J. Rosenow, R. Alligier, and H. Fricke, "Prediction of the propagation of trajectory uncertainty for climbing aircraft," in *39th AIAA/IEEE Digital Avionics Systems Conference*, (San Antonio, TX), 2020.
[17] J. Sun, H. A. Blom, J. Ellerbroek, and J. M. Hoekstra, "Aircraft Mass and Thrust Estimation Using Recursive Bayesian Method," in *8th International Conference on Research in Air Transportation (ICRAT2018)*, (Castelldefels), 2018.
[18] Q. Zheng and Y. Zhao, "Modeling Wind Uncertainties for Stochastic Trajectory Synthesis," in *11th AIAA Aviation Technology, Integration, and Operations (ATIO) Conference*, (Virginia Beach, VA), American Institute of Aeronautics and Astronautics, Sept. 2011.
[19] J. Cheung, A. Hally, J. Heijstek, A. Marsman, and J.-L. Brenguier, "Recommendations on trajectory selection in flight planning based on weather uncertainty," in *Fifth SESAR Innovation Days*, 2015.
[20] J. Wan, H. Zhang, F. Liu, W. Lv, and Y. Zhao, "Optimization of aircraft climb trajectory considering environmental impact under RTA constraints," *Journal of Advanced Transportation*, vol. 2020, p. 2738517, Aug 2020.
[21] S. Lloyd, "Least squares quantization in PCM," *IEEE Transactions on Information Theory*, vol. 28, pp. 129–137, Mar. 1982.
[22] Z. Wang, A. Liang, and D. Delahaye, "Short-term 4D Trajectory Prediction Using Machine Learning Methods," in *7th SESAR Innovation Days*, (Belgrade), Nov. 2017.
[23] X. Olive and J. Morio, "Trajectory clustering of air traffic flows around airports," *Aerospace Science and Technology*, vol. 84, pp. 776–781, Jan. 2019.
[24] M. Gariel, A. N. Srivastava, and E. Feron, "Trajectory Clustering and an Application to Airspace Monitoring," *IEEE Transactions on Intelligent Transportation Systems*, vol. 12, pp. 1511–1524, Dec. 2011.
[25] L. Basora, J. Morio, and C. Mailhot, "A Trajectory Clustering Framework to Analyse Air Traffic Flows," in *7th SESAR Innovation Days*, (Belgrade), 2017.
[26] S. J. Corrado, T. G. Puranik, O. J. Pinon, and D. N. Mavris, "Trajectory Clustering within the Terminal Airspace Utilizing a Weighted Distance Function," *Proceedings*, vol. 59, p. 7, Dec. 2020.
[27] X. Olive, L. Basora, B. Viry, and R. Alligier, "Deep Trajectory Clustering with Autoencoders," in *International Conference for Research in Air Transportation (ICRAT 2020)*, (Tampa, FL), Aug. 2020.
[28] E. Salaün, M. Gariel, A. E. Vela, and E. Feron, "Aircraft Proximity Maps Based on Data-Driven Flow Modeling," *Journal of Guidance, Control, and Dynamics*, vol. 35, pp. 563–577, Mar. 2012.
[29] W. J. Eerland, S. Box, and A. Sóbester, "Modeling the dispersion of aircraft trajectories using gaussian processes," *Journal of Guidance, Control, and Dynamics*, vol. 39, no. 12, pp. 2661–2672, 2016.
[30] M. Murça, R. Delaura, R. Hansman, R. Jordan, T. Reynolds, and H. Balakrishnan, *Trajectory Clustering and Classification for Characterization of Air Traffic Flows*.
[31] Joint Planning and Development Office, Next Generation Air Transportation System, "Concept of Operations for the Next Generation Air Transportation System, Version 3.2," tech. rep., 2011.
[32] M. Lindner, J. Rosenow, T. Zeh, and H. Fricke, "In-flight aircraft trajectory optimization within corridors defined by ensemble weather forecasts," *Aerospace*, vol. 7, no. 10, 2020.
[33] M. Lindner, T. Zeh, and H. Fricke, "Reoptimizaton of 4D-Flight Trajectories During Flight Considering Forecast Uncertainties," in *Deutscher Luft- Und Raumfahrtkongress (DLRK)*, (Friedrichshafen), 2018.
[34] International Civil Aviation Organization, "Continuous descent operations (CDO) Manual," Tech. Rep. Doc 9931 AN/476, Montreal, 2010.
[35] N. Takeichi and Y. Abumi, "Benefit optimization and operational requirement of flow corridor in japanese airspace," *Proceedings of the Institution of Mechanical Engineers, Part G: Journal of Aerospace Engineering*, vol. 230, 11 2015.
[36] A. Errico and V. D. Vito, *Aircraft operating technique for efficient sequencing arrival enabling environmental benefits through CDO in TMA*. 2019.
[37] R. Sáez, X. Prats, T. Polishchuk, V. Polishchuk, and C. Schmidt, "Automation for separation with continuous descent operations: Dynamic aircraft arrival routes," *Journal of Air Transportation*, vol. 28, no. 4, pp. 144–154, 2020.
[38] J. Zhou, S. Cafieri, D. Delahaye, and M. Sbihi, "Optimization-based design of departure and arrival routes in terminal maneuvering area," *Journal of Guidance, Control, and Dynamics*, vol. 40, no. 11, pp. 2889–2904, 2017.
[39] V. Ho-Huu, S. Hartjes, H. Visser, and R. Curran, "An optimization framework for route design and allocation of aircraft to multiple departure routes," *Transportation Research Part D Transport and Environment*, vol. 76, 10 2019.
[40] J. Chevalier, D. Delahaye, M. Sbihi, and P. Marechal, "Departure and arrival routes optimization near large airports," *Aerospace*, vol. 6, p. 80, 07 2019.
[41] J. Rosenow and H. Fricke, "Flight performance modeling to optimize trajectories," in *Deutscher Luft- Und Raumfahrtkongress (DLRK)*, 2016.
[42] T. Vincenty, "Direct and inverse solutions of geodesics on the ellipsoid with application of nested equations," *Survey Review*, vol. 23, no. 176, pp. 88–93, 1975.
[43] P. E. Hart, N. J. Nilsson, and B. Raphael, "A formal basis for the heuristic determination of minimum cost paths," *IEEE Transactions on Systems Science and Cybernetics*, vol. 4, no. 2, pp. 100–107, 1968.
[44] International Civil Aviation Organization, "2016–2030 Global Air Navigation Plan, Doc 9750-AN/963, 5th Edition," tech. rep., 2016.
[45] DFS Deutsche Flugsicherung, "AIP Germany Part AD, Airport Munich (EDDM), AMDT 03/20," 2021.
[46] NOAA National Centers for Environmental Prediction (NCEP), "NOAA/NCEP Global Forecast System (GFS) Atmospheric Model." online, 01 2021.

Martin Lindner studied Aviation Technology and Logistics at Technische Universität Dresden (TUD) from 2007-2013. At the same Institute, he then began working on projects in the field of flight trajectory optimization and flight performance modeling as a research associate until now. In his intended doctoral thesis, he focuses on the goal of making aircraft rotation schedules less vulnerable to delays.

Thomas Zeh studied Aviation Technology and Logistics at TUD, where he became a graduate engineer in 2015. Then, he worked on aeronautical studies and safety management systems at GfL Gesellschaft für Luftverkehrsforschung mbH. In 2017, he returned to TUD as a research associate in the area of trajectory optimization and flight performance modeling. His doctoral thesis research focuses on trajectory prediction under uncertainty.

Hannes Braßel is a research associate and Ph.D. student in Transport Engineering at the Institute of Aviation and Logistics, TUD. He graduated from TUD with a Diploma degree in Transport Engineering (2018). During his studies, he worked as a research assistant in the DLR student laboratory and as a student trainee in the German Aerospace Center, Institute of Flight Guidance, Controller Assistance.

Hartmut Fricke studied Aeronautics and Astronautics at TU Berlin from 1985-1991 where he also received his doctorate in ATM. In 2001 he finished his habilitation on "Integrated Collision Risk Modeling for airborne and ground based systems". Since December 2001, he is a professor for Aviation Technologies and Logistics at TUD. In 2006 he was appointed Member of the Scientific Advisory Board to the German Federal Minister of Transport. He is a member of various journal review committees. In 2012 he was elected scientific expert to DFG. In 2013 he became SESAR External Expert.